applied optics

Picosecond and femtosecond asymmetric switching using a semiconductor optical amplifier-based Mach–Zehnder interferometer

Yaser Khorrami,[1] Vahid Ahmadi,[1,*] Mohammad Razaghi,[2] and Narottam Das[3]

[1]Department of Electrical and Computer Engineering, Tarbiat Modares University, Tehran, Iran
[2]Department of Engineering, University of Kurdistan, Sanandaj, Iran
[3]School of Mechanical and Electrical Engineering, University of Southern Queensland, Toowoomba, West Street, QLD 4350, Australia
*Corresponding author: v_ahmadi@modares.ac.ir

Received 16 October 2017; revised 16 January 2018; accepted 26 January 2018; posted 29 January 2018 (Doc. ID 309282); published 27 February 2018

In this paper, we numerically analyze nonlinear asymmetric switching using a semiconductor optical amplifier (SOA) phase-shifter-based Mach–Zehnder interferometer (MZI), for the first time, to the best of our knowledge. The self-phase modulation (SPM) effect and nonlinear phase shift in each MZI arm are investigated for different input pulse intensities and linear gains in both picosecond and femtosecond regimes. The input light signal is split unequally over the two arms, where SOAs are placed and act as nonlinear phase shifters in each arm. The finite difference beam propagation method is used to solve the modified nonlinear Schrodinger equation to analyze the wave propagation. In this work, the main nonlinear effects in SOA, such as group velocity dispersion, Kerr effect, two-photon absorption, carrier heating, and spectral hole burning, are considered. Furthermore, the effect of SPM on distortion of the pulse shape and its spectrum, which can be used for pulse shaping in a picosecond-switching scheme, is studied. We depicted red and blue shifts that each pulse experiences in the process of switching in picosecond and femtosecond regimes, respectively. Based on the results for sub-picosecond input pulses, by controlling the bias current level in the MZI arms, the pulse distortion due to nonlinear effects of SOAs can be decreased at the switch output port, and symmetric pulse can be obtained. Switching with higher speed is possible in bulk SOAs in the femtosecond regime using asymmetric MZI-switching structure.

OCIS codes: (130.4815) Optical switching devices; (320.2250) Femtosecond phenomena; (190.0190) Nonlinear optics; (250.5980) Semiconductor optical amplifiers.

https://doi.org/10.1364/AO.57.001634

1. INTRODUCTION

The semiconductor optical amplifier (SOA) as a key component in high-speed optical communication systems has been of great interest in recent years. By using the rate equation model, the nonlinear gain and phase dynamics of this device can be described in a phenomenological way. Ultra-short optical pulse shaping using the SOA has been reported earlier [1,2]. Among interferometric structures, the SOA-based Mach–Zehnder interferometer (MZI) using cross-phase modulation (XPM) is a promising candidate due to its attractive features of low energy requirement, simplicity, compactness, and stability [3–5]. Another switching technique is based on the self-phase modulation (SPM) phenomena of SOA [6]. If the input signal is split unequally over the interferometer arms, the two SOAs operate in different regimes, yielding a phase difference between the two signals that propagates in each arm. Because of the finite carrier lifetime, the leading edge of the pulse experiences a different phase shift relative to the lagging edge. The SPM will change the pulse shape as well as its spectrum. The SPM pulse-narrowing effect can be used as a dispersion compensator to reshape the pulse broadening resulting from chromatic dispersion of optical fiber. This type of device has great potential for increasing the capacity of high-speed long-haul fiber links [7].

Heretofore, a new structure of the SOA-based Sagnac interferometer self-switch [8] and also the Tb/s all-optical symmetric switch using SOA-based MZI are presented [9].

In this paper, we have analyzed nonlinear asymmetric switching (self-switching, SS) using the SOA phase-shifter-based MZI, for the first time, to the best of the authors' knowledge. Furthermore, the SPM effect and nonlinear phase shift in each arm for different values of input intensities, linear gain,

and power splitting ratio are investigated in both picosecond and femtosecond regimes with the finite difference beam propagation method (FD-BPM).

The SS technique can be used in some applications, such as a pattern-effect compensator, 2R-regenerator, and low-loss optical combiner circuits [10–12]. The SS in MZI based on SOA, unlike the symmetric MZI scheme, does not need any extra pulses and consumes low power [6] and, unlike the nonlinear polarization switch (NPS), has the advantage to be polarization insensitive [12].

This paper is organized as follows: Section 1 is an introduction. The theory of the SS is scheme described in Section 2. Section 3 presents the SOA model, and Section 4 describes the simulation results and discussion. Finally, the conclusion is in Section 5.

2. THEORY OF SELF-SWITCHING SCHEME

A schematic diagram of a self-switching configuration with unequal power splitting is shown in Fig. 1.

An arbitrary signal with specific data rate is launched at one of the input ports that is divided asymmetrically into each arm by the coupler. In this work, multimode interference (MMI) couplers are used to split/combine the signals. The MMI coupler is utilized to divide the input signal unequally between arms using splitting/coupling ratio parameters that can be adjusted. Figure 1 shows the bias currents for the SOA1 and SOA2 as indicated with I_1 and I_2, respectively, which are equal here to $I_1(= 200$ mA). In the high optical power arm, the SOA experiences pronounced SPM, causing changes in both the gain and the refractive index as a function of optical input intensity. MZI due to its interferometric structure compares the phase difference between the two arms. Such a phase difference can be controlled by the bias currents and by varying the input power at each amplifier that enables SS [12]. The optical input signal is injected into one of the input ports (here, port 1 as shown in Fig. 1). The power splitting ratios in input and output couplers are X and Y, respectively. By setting $X < 0.5$, a nonlinear phase shift is induced to the signal in the high-optical-power arm (here, SOA2), which experiences (1-X) percent of injection power. In the low-power arm, the SOA is operating in an unsaturated regime (here, SOA1), so both gain and refractive index changes become negligible. The maximum transmission signal from port 1 to the switched port (denoted by S-port in Fig. 1) can be obtained if the induced nonlinear phase shift between the arms equals π i.e., 180°. If $Y = X$, the output power at the switched port can be written as

$$P_{\text{out}}(t) = \text{TF}(t) \cdot P_{\text{in}}(t), \tag{1}$$

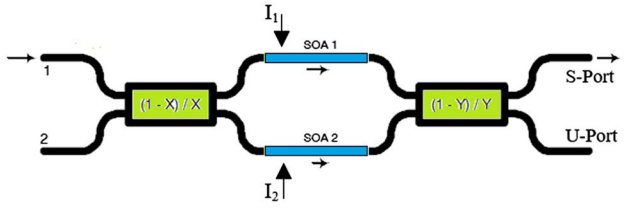

Fig. 1. Schematic diagram of MZI-based switch using SOA with unequal power distribution due to 2 × 2 MMI coupler.

where $P_{\text{out}}(t)$ and $P_{\text{in}}(t)$ are the output power from S-port and input power injected into port 1, respectively. TF(t) is the transfer function of the proposed switch as expressed by [12]:

$$\text{TF}(t) = X \cdot Y \cdot G_1(t) + (1-X) \cdot (1-Y) \cdot G_2(t) - 2\sqrt{X \cdot Y \cdot (1-X) \cdot (1-Y) \cdot G_1(t) \cdot G_2(t)} \cos[\Delta\phi_{\text{NL}}(t)], \tag{2}$$

where $G_1(t)$ and $G_2(t)$ are the gain of SOA1 and SOA2, respectively. $\Delta\phi_{\text{NL}}$ is the total phase difference accumulated by the optical signals as given by [12]

$$\Delta\phi_{\text{NL}}(t) = \Delta\phi_1(t) - \Delta\phi_2(t) = (-\alpha/2) \cdot \ln(G_2/G_1), \tag{3}$$

where $\Delta\phi_{\text{NL}}(t)$ is the time-delayed phase shift in the two arms that are related to the gain of each arm via the linewidth enhancement factor (α). The linewidth enhancement factor is defined as the ratio of the variations of the real and imaginary parts of the refractive index, which is used to describe the relation between phase shift and the gain. In nonlinear analysis of SOA, we should consider the effect of the linewidth enhancement factor due to carrier depletion and carrier heating as the most effective nonlinear parameters that affect the refractive index.

3. SOA MODEL

The following modified nonlinear Schrödinger equation (MNSE) [13,14] is used for the analysis of SOAs and the characteristics of SS:

$$\left[\frac{\partial}{\partial z} - \frac{i}{2}\beta_2\frac{\partial^2}{\partial\tau^2} + \frac{\gamma}{2} + \left(\frac{\gamma_{2P}}{2} + ib_2\right)|V(\tau,z)|^2\right]V(\tau,z) = \left\{\frac{1}{2}g_N(\tau)\left[\frac{1}{f(\tau)} + i\alpha_N\right] + \frac{1}{2}\Delta g_T(\tau)(1+i\alpha_T) - i\frac{1}{2}\frac{\partial g(\tau,\omega)}{\partial\omega}\bigg|_{\omega_0}\frac{\partial}{\partial\tau} - \frac{1}{4}\frac{\partial^2 g(\tau,\omega)}{\partial\omega^2}\bigg|_{\omega_0}\frac{\partial^2}{\partial\tau^2}\right\}V(\tau,z), \tag{4}$$

where

$$g_N(\tau) = g_0 \exp\left(-\frac{1}{W_s}\int_{-\infty}^{\tau} e^{-s/\tau_s}|V(s)|^2 ds\right), \tag{5}$$

$$f(\tau) = 1 + \frac{1}{\tau_{\text{shb}}P_{\text{shb}}}\int_{-\infty}^{+\infty} u(s)e^{-s/\tau_{\text{shb}}}|V(\tau-s)|^2 ds, \tag{6}$$

$$\Delta g_T(\tau) = -h_1\int_{-\infty}^{+\infty} u(s)e^{-s/\tau_{\text{ch}}}(1-e^{-s/\tau_{\text{shb}}})|V(\tau-s)|^2 - h_2\int_{-\infty}^{\infty} u(s)e^{-s/\tau_{\text{ch}}}(1-e^{-s/\tau_{\text{shb}}})|V(\tau-s)|^4 ds, \tag{7}$$

$$\frac{\partial g(\tau,\omega)}{\partial\omega}\bigg|_{\omega_0} = A_1 + B_1[g_0 - g(\tau,\omega_0)], \tag{8}$$

$$\frac{\partial^2 g(\tau,\omega)}{\partial\omega^2}\bigg|_{\omega_0} = A_2 + B_2[g_0 - g(\tau,\omega_0)], \tag{9}$$

$$g(\tau,\omega_0) = g_N(\tau,\omega_0)/f(\tau) + \Delta g_T(\tau,\omega_0). \tag{10}$$

Time frame $\tau(=t-z/\nu_g)$ propagates with group velocity ν_g at the center frequency of an optical pulse. The slowly varying envelope approximation is used in Eq. (4). Here, $V(\tau,z)$ is the time domain complex envelope function of an optical pulse, $|V(\tau,z)|^2$ corresponds to the optical power, β_2 is the group velocity dispersion (GVD), γ is linear loss, γ_{2P} is the two-photon absorption (TPA) coefficient, $b_2(=\omega_0 n_2/cA)$ is the instantaneous SPM term due to the instantaneous nonlinear Kerr effect n_2, and $\omega_0(=2\pi f_0)$ is the center angular frequency of the pulse. Also, c is the velocity of light in vacuum, A is the effective area of the active region, $g_N(\tau)$ is the saturated gain due to carrier depletion [Eq. (5)], and g_0 is the linear gain. W_0 is the saturation energy, τ_s is the carrier lifetime, $f(\tau)$ is the SHB function [Eq. (6)]. P_{SHB} is the spectral hole burning (SHB) saturation power, τ_{SHB} is the SHB relaxation time, and α_N and α_T are the linewidth enhancement factors associated with the gain changes due to carrier depletion and carrier heating (CH). $\Delta g_T(\tau)$ is the resulting gain change due to CH and TPA [Eq. (7)], u(s) is the unit step function, τ_{CH} is the CH relaxation time, h_1 is the contribution of stimulated emission and free carrier absorption to CH gain reduction, h_2 is the contribution of TPA, A_1 and A_2 are the slope and curvature of linear gain at ω_0, and B_1 and B_2 are constants describing changes in these quantities with saturation [Eqs. (8) and (9)]. The gain spectrum of an SOA can be approximated by the following second-order Taylor expansion in ω:

$$g(\tau,\omega)=g(\tau,\omega_0)+\Delta\omega\left.\frac{\partial g(\tau,\omega)}{\partial\omega}\right|_{\omega_0}+\frac{(\Delta\omega)^2}{2}\left.\frac{\partial^2 g(\tau,\omega)}{\partial\omega^2}\right|_{\omega_0}. \tag{11}$$

Table 1. Parameters Used in Simulation [15,16]

Symbol	Quantity	Values (units)
L	SOA cavity length	500 μm
A	Effective area	5 μm^2
f_0	Center frequency of the pulse	193.5 THz
g_0	Linear gain	90 cm^{-1}
β_2	Group velocity dispersion	0.045 $ps^2\,cm^{-1}$
W_s	Saturation energy	10 pj
α_N	Linewidth enhancement factor due to carrier depletion	7
α_T	Linewidth enhancement factor due to CH	1
h_1	Contribution of stimulated emission and free carrier absorption to CH gain reduction	0.3 $cm^{-1}\,pj^{-1}$
h_2	Contribution of TPA	300 $fs\,cm^{-1}\,pj^{-2}$
τ_s	Carrier lifetime	500 ps
τ_{CH}	CH relaxation time	800 fs
τ_{shb}	Spectral hole burning relaxation time	150 fs
P_{SHB}	SHB relaxation power	11.32 W
γ	Linear loss	15 cm^{-1}
n_2	Instantaneous nonlinear Kerr effect	−0.6 $cm^2\,TW^{-1}$
γ_{2P}	TPA coefficient	1.6 $cm^{-1}\,W^{-1}$
$A_{1,2}$	Parameters describing second-order	0.8 $fs\,\mu m^{-1}$, −150 fs
$B_{1,2}$	Taylor expansion of dynamic gain spectrum	−150 $fs^2\,\mu m^{-1}$, 0 fs^2

The coefficients $\frac{\partial g(\tau,\omega)}{\partial\omega}|_{\omega_0}$ and $\frac{\partial^2 g(\tau,\omega)}{\partial\omega^2}|_{\omega_0}$ are related to A_1, B_1, A_2, and B_2 by Eqs. (8) and (9). The time derivative terms in the MNSE have been replaced with the central-difference approximation in order to solve this equation by the FD-BPM [13,14]. The parameters are listed in Table 1.

4. SIMULATION RESULTS AND DISCUSSION

A. Picosecond Scheme

The simulation is performed for the InGaAsP/InP material system. The SOAs have cavity lengths of 500 μm with optical signal at the wavelength of 1.55 μm. For the couplers, MMI devices are chosen because of their compact design and polarization insensitivity [6]. We have considered the linear gain as a variable in our simulation. We can determine each amplifier current from Eq. (12) for various amounts of the confinement factor (Γ), differential gain (a), carrier density (N_0), and current required for the transparency (I_0):

$$g_0=\Gamma a N_0(I/I_0-1). \tag{12}$$

All pulse propagation simulations are performed at the injection current of 200 mA corresponding to a linear gain of 90 cm^{-1} [16].

In the following simulation, the input power splitting ratio is taken as $X=0.15$ and the $sech^2$ pulses with 10 ps full width at half-maximum (FWHM), which are Fourier transform limited. The variation of phase difference and its cosine with time is summarized in Fig. 2. For differential nonlinear phase shift between two arms, Fig. 2(Right) depicts that the phase difference between two arms equals π at pick pulse ($t=0$), and there is optimal phase difference, which causes maximum value in Fig. 2(Left) at the same time. This value for cosine function creates maximum transfer function from Eq. (2).

Figure 3(a) shows the gain spectra given by a second-order Taylor expansion for the pulse center frequency with derivatives of $g(\tau\cdot\omega)$. The solid and dashed lines show the unsaturated and saturated gain spectrum for SOA1 and SOA2, respectively. As depicted, the linear gain (g_0) at ω_0 for SOA1 and SOA2 are 90 cm^{-1} and 35 cm^{-1}, respectively. Figure 3(b) shows the gain of each amplifier for input pulse versus time characteristics. The dashed line is the saturated temporal gain in the high-power arm (SOA2 in this case).

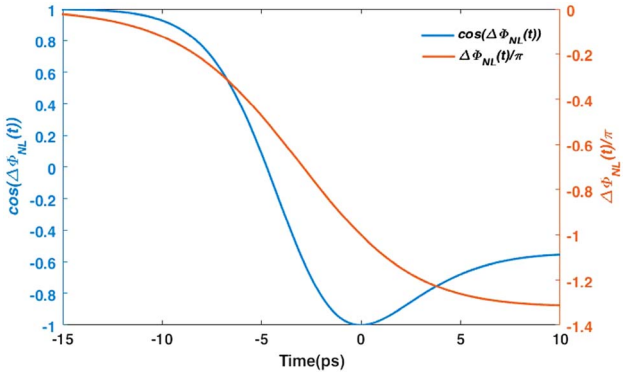

Fig. 2. (Right) Variation of phase difference between two arms of MZI, which is equal to π at $t=0$. (Left) Time variation of $\cos(\Delta\phi_{\mathrm{NL}}(t))$.

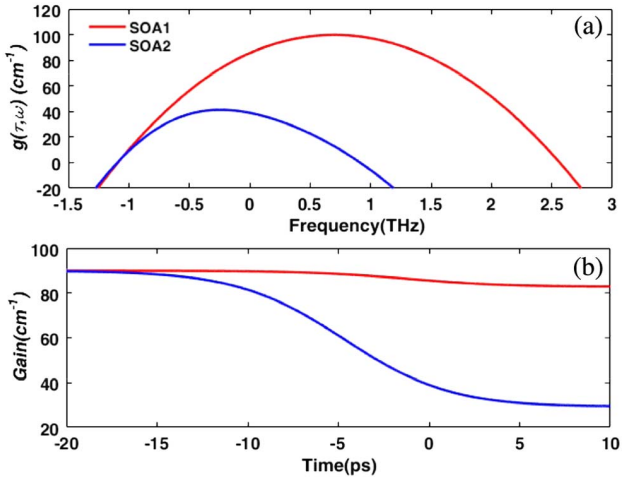

Fig. 3. (a) Gain spectra in each arm. (b) Gain variation versus time for each arm.

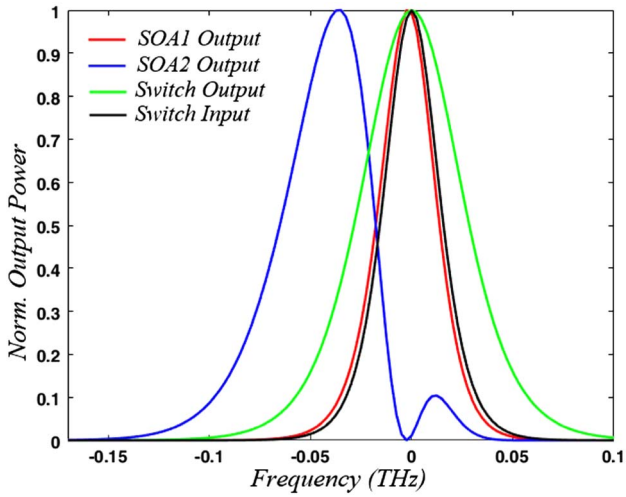

Fig. 5. Output pulse spectrum of each amplifier; switch input and output.

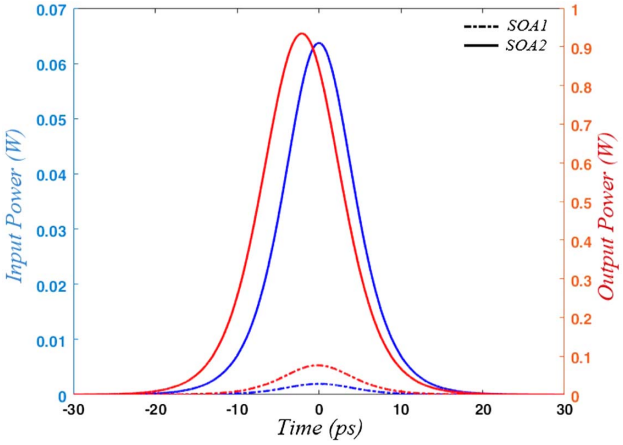

Fig. 4. (Left) Input pulse shape of each amplifier. (Right) Output pulse shape of each amplifier.

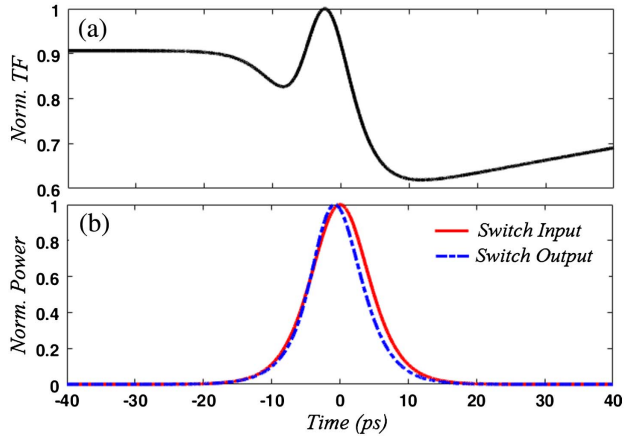

Fig. 6. (a) Normalized transfer function of switch. (b) Normalized input and output power of switch.

Figures 4(Left and Right) depict the input and output pulse shapes of amplifiers, respectively. The dashed line in Fig. 4 is SOA1, and the solid line is SOA2. Both input pulses are centered symmetrically at $t = 0$. But, as shown in Fig. 4(Right), the output pulse is distorted, so that its peak position is shifted to the negative times zone (i.e., leading edge). This temporal distortion is due to nonlinear effects, especially SPM, and is little for low input powers, as shown in Fig. 4(Right). The output spectra of two SOAs and switch output are shown in Fig. 5. It has been shown that the red shift occurs because of the strong SPM effect of second SOA.

The oscillatory behavior of the SOA2 output spectrum is shown in Fig. 5, which is due to destructive interference of the high-power propagated field in the SOA cavity.

Figure 6 depicts transfer function and switch input and output pulse shapes. Transfer function in Fig. 6(a) determines the width of switch output, which in turn is dependent on gain and phase difference between arms. The SPM mostly affects the high-optical-power arm, but this nonlinearity in overall output of MZI is negligible, as illustrated in Fig. 6(b). Therefore, a little SPM effect can appear in the switch output. The presented model is developed to analyze the nonlinear effect of each SOA on MZI in the SS scheme.

Figure 7 shows the MZI temporal output power for different values of linear gain. For pulses with multi-ten picosecond pulse widths, the effective nonlinear effect is SPM [17]. More pulse widths and more injected energy increase carrier depletion, which is the main reason for SPM in the picosecond regime. This phenomenon becomes more influential by increasing linear gain as described. In this condition, the leading edge of the input pulse experiences unchanged gain and is linearly amplified, but for the trailing edge, the gain is saturated, and the amplification becomes nonlinear. Figure 7 also shows that one can have a pulse-shaping feature besides the switching simultaneously.

MZI transfer function and output power for different values of input power injection are illustrated in Fig. 8. As it is shown, the output power experiences more chirp by increasing the

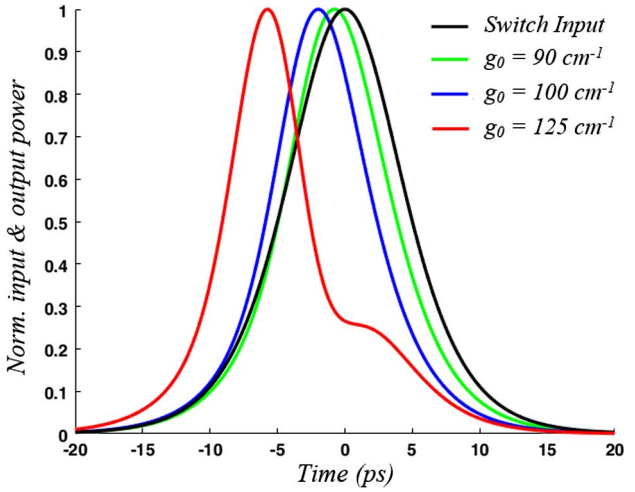

Fig. 7. Normalized input and output power for various amounts of g_0, 90, 100, and 125 (cm^{-1}).

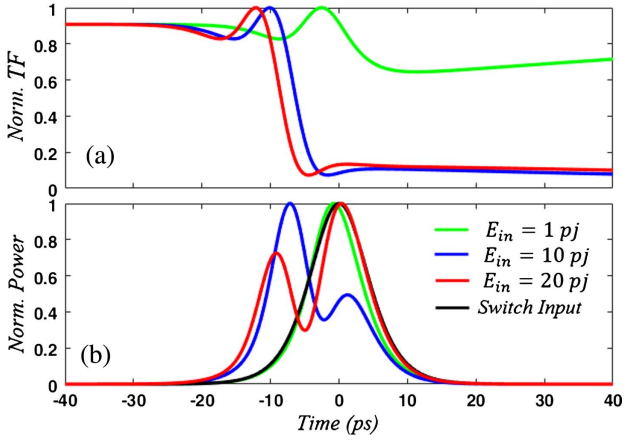

Fig. 8. (a) MZI transfer function for different values of power injection (1 pJ, 10 pJ, and 20 pJ). (b) Input and output power of MZI for the same values of power injection.

input power because of intense carrier depletion in the high-power regime. Gain saturation distorts the trailing edge of the input signal, except for 20 pJ input energy. The main reason for pulse shape inversion for 20 pJ in comparison with 1 and 10 pJ is that the recent injection power (20 pJ) is much higher than SOA saturation energy ($W_s = 10$ pJ).

B. Femtosecond Scheme

Fast mechanisms such as CH and SHB in SOA in the short pulse amplification regimes are very important [18,19]. To investigate the effects of such phenomena, the SS mechanism is simulated with femtosecond input pulses. In this case, the input pulse energy of 50 fJ with FWHM of 180 fs is used. Figure 9(a) shows the optical spectrum of each SOA and MZI output. Unlike the picosecond regime, blue shift occurs for both SOAs' output, and the SOAs' output pulse peaks have shifted to the higher frequencies. The blue shift in the femtosecond regime is due to the SHB and CH. Unlike SPM, because of short pulse

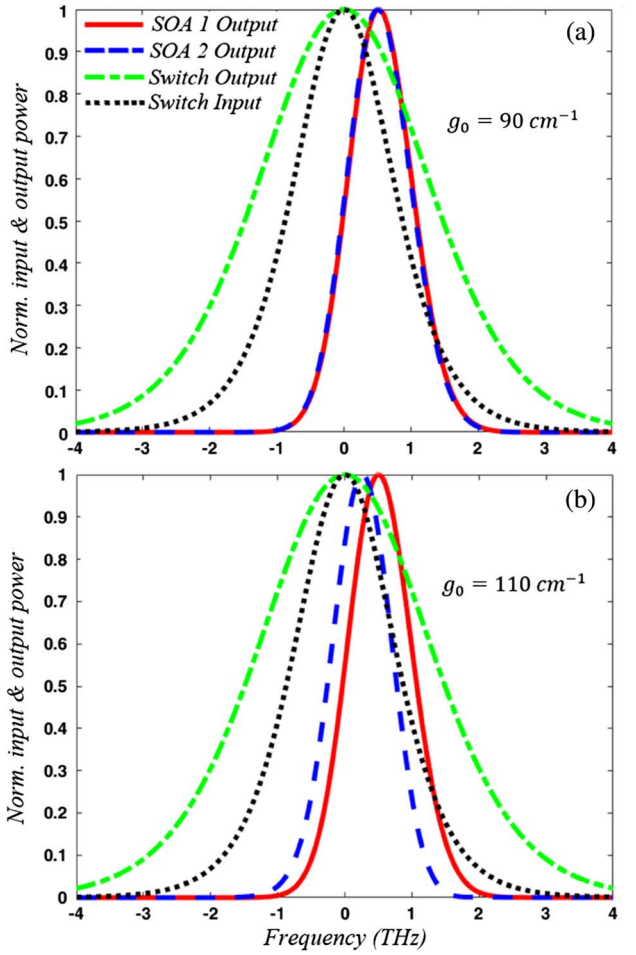

Fig. 9. Output spectrum of each SOA; switch input and output for (a) $g_0 = 90\ cm^{-1}$ and (b) $g_0 = 110\ cm^{-1}$.

widths, the SHB and CH phenomena impose a positive chirp on the propagated pulse. So SOAs become saturated, caused by the recent nonlinear intra-band effects. In the femtosecond scheme, unequally feeding intensity into the MZI arms and high input pulse energy (with respect to its short width) heated the carriers, and hole burning takes place. Figure 9(a) also shows that there is no red or blue shift effect in the output spectrum of MZI. Figure 9(b) shows blue shift of each SOA's output spectrum for linear gain of $g_0 = 110\ cm^{-1}$. There is also no blue shift for the overall output spectrum of switch, but the blue shift effect of SOA2 output becomes smaller, compared to the case shown in Fig. 9(a).

The SPM takes place by carrier depletion as the inter-band effect. Therefore, SPM has pronounced effect due to the wide range of pulse widths or high input power for picosecond regime. In the picosecond regime, carrier depletion creates the red shift. Similarly, in the femtosecond regime, when we increase the value of g_0 from 90 cm^{-1} to 110 cm^{-1}, the carrier rate increases in conduction and valence bands, and more negligible SPM becomes apparent in Fig. 9(b) in comparison to Fig. 9(a).

Therefore, the SOA2 output spectrum experiences few red shifts due to inter-band effects and more blue shift due to band filling caused by intra-band effects, such as SHB and CH,

which have fast relaxation time (50 fs–700 fs). Relaxation time of carrier depletion is longer than SHB and CH relaxation time, so the red shift of the SOA2 output pulse occurs after blue shift (move to right on frequency axis) of this pulse in Fig. 9(b). The SOA1 output spectrum pulse is still in higher frequencies (blue shift) without any backward movement (red shift), which shows no SPM becomes apparent in the first SOA because of less input power injection in SOA1 with respect to its short pulse width.

5. CONCLUSION

We have numerically analyzed the asymmetric switching mechanism in SOA-based MZI with unequal distribution of input optical signal over MZI arms. We used FD-BPM for the simulation of SOA. With the SOA length of 500 μm, we observed large nonlinearity with the numerical simulation. Furthermore, we analyzed the SPM effect in the picosecond regime on the MZI SS mechanism for 10 ps input pulses as a main nonlinear effect. We found that the output pulses in the picosecond state compressed, and this effect using various amounts of linear gain can be used for pulse shaping. We observed that there is only red shift in the picosecond regime due to inter-band effects, but there are both red and blue shifts in the femtosecond regime for the SOAs' output, due to the intraband effects that can be seen. It was shown that for picosecond input pulses, based on the bias current of the SOAs in MZI arms, different amounts of pulse compression can be achieved. It was depicted that for picosecond pulses due to the SPM effect, the switch output pulse spectrum experiences red shift, while for sub-picosecond input pulses, due to the ultrahigh speed nonlinear effect, the switch output pulse is blue shifted. By increasing the bias current level of SOAs in MZI arms, this blue shift can be compensated. Therefore, switching with higher speed is possible in bulk SOAs in a femtosecond differential asymmetric MZI SS scheme.

REFERENCES

1. H. Aghajanpour, V. Ahmadi, and M. Razaghi, "Ultra-short optical pulse shaping using semiconductor optical amplifier," Opt. Laser Technol. **41**, 654–658 (2009).
2. S. R. Hosseini, M. Razaghi, and N. K. Das, "Analysis of non-linear refractive index influences on four-wave mixing conversion efficiency in semiconductor optical amplifiers," Opt. Laser Technol. **44**, 528–533 (2012).
3. C. Reis, T. Chattopadhyay, G. Parca, R. Dionísio, P. André, and A. Teixeira, "All-optical multifunctional logic operations using simultaneously both interferometric output ports in a symmetric SOA-MZI," Opt. Laser Technol. **68**, 175–181 (2015).
4. T. Chattopadhyay, C. Reis, P. André, and A. Teixeira, "Theoretical analysis of all-optical clocked D flip-flop using a single SOA assisted symmetric MZI," Opt. Commun. **285**, 2266–2275 (2012).
5. C. Janz and B. Lavigne, "Low penalty 10 Gb/s operation of polarization-insensitive Mach–Zehnder wavelength converters based on bulk-tensile active material," in *Optical Fiber Communication Conference* (1998), pp. 101–102.
6. E. Patent and J. Van der Tol, "Self-switching in Mach–Zehnder interferometers with SOA phase shifters," IEEE Photon. Technol. Lett. **17**, 2301–2303 (2005).
7. M. J. Connelly, *Semiconductor Optical Amplifier* (Kluwer Academic, 2004).
8. M. Jamali, V. Ahmadi, and M. Razaghi, "Optical self-switching based on a semiconductor optical-amplifier-assisted Sagnac interferometer," J. Opt. Soc. Am. B **30**, 2576–2583 (2013).
9. Y. Khorrami, V. Ahmadi, and M. Razaghi, "Tb/s all-optical nonlinear switching using SOA based Mach–Zehnder interferometer," Sci. Iran. D **21**, 843–852 (2014).
10. E. A. Patent and J. J. G. M. van der Tol, "A pattern effect compensator," in *IEEE/LEOS Symposium* (Benelux Chapter, 2001), pp. 233–236.
11. K. I. Kang, T. G. Chang, I. Glesk, and P. R. Prucnal, "Comparison of Sagnac and Mach–Zehnder ultrafast all-optical interferometric switches based on a semiconductor resonant nonlinearity," Appl. Opt. **35**, 417–426 (1996).
12. S. Gupta, N. Calabretta, M. Presi, and G. Contestabile, "Operational equivalence of self-switching in MZI and nonlinear polarization switches based on SOAs," IEEE J. Quantum Electron. **14**, 779–788 (2008).
13. N. K. Das, Y. Yamayoshi, and H. Kawaguchi, "Analysis of optical phase-conjugate characteristics of picosecond four-wave mixing signals in semiconductor optical amplifiers," IEEE J. Quantum Electron. **36**, 1184–1192 (2000).
14. N. K. Das, Y. Yamayoshi, T. Kawazoe, and H. Kawaguchi, "Analysis of all-optical DEMUX based on four-wave mixing in SOAs," IEEE J. Lightwave Technol. **19**, 237–246 (2001).
15. R. P. Schreieck, M. H. Kwakernaak, H. Jäckel, and H. Melchior, "All-optical switching at multi-100-Gb/s data rates with Mach–Zehnder interferometer switches," IEEE J. Quantum Electron. **38**, 1053–1061 (2002).
16. Y. H. Kao, I. V. Goltser, M. Jiang, M. N. Islam, and G. Raybon, "Gain dispersion induced subpicosecond pulse breakup in a fiber and semiconductor laser amplifier combined system," Appl. Phys. Lett. **69**, 4221–4223 (1996).
17. Y. V. Zachinyaev and K. E. Rumyantsev, "Self-phase modulation based chirp generator," in *IEEE Radar Conference* (2016).
18. S. Bischoff, "Comparison of all optical co and counter propagating high speed signal processing in SOA based MZI," Opt. Quantum Electron. **33**, 907–926 (2001).
19. P. Borri, W. Langbein, J. M. Hvam, F. Heinrichsdorff, M. H. Mao, and D. Bimberg, "Spectral hole-burning and carrier-heating dynamics in InGaAs quantum-dot amplifiers," IEEE J. Quantum Electron. **6**, 544–551 (2000).